

UCLA

UCLA Previously Published Works

Title

ZIP8 A391T Crohns Disease-Linked Risk Variant Induces Colonic Metal Ion Dyshomeostasis, Microbiome Compositional Shifts, and Inflammation.

Permalink

<https://escholarship.org/uc/item/6nb7n5bg>

Journal

Digestive Diseases and Sciences, 69(10)

Authors

Yang, Julianne
Zhao, Matthew
Chernikova, Diana
[et al.](#)

Publication Date

2024-10-01

DOI

10.1007/s10620-024-08647-8

Peer reviewed



ZIP8 A391T Crohn's Disease-Linked Risk Variant Induces Colonic Metal Ion Dyshomeostasis, Microbiome Compositional Shifts, and Inflammation

Julianne C. Yang¹ · Matthew Zhao^{1,2} · Diana Chernikova^{1,3} · Nerea Arias-Jayo¹ · Yi Zhou^{1,4} · Jamilla Situ¹ · Arjun Gutta¹ · Candace Chang¹ · Fengting Liang¹ · Venu Lagishetty¹ · Jonathan P. Jacobs^{1,5,6}

Received: 20 August 2024 / Accepted: 10 September 2024 / Published online: 25 September 2024
This is a U.S. Government work and not under copyright protection in the US; foreign copyright protection may apply 2024

Abstract

Background The pathogenesis of Crohn's disease involves genetic and environmental factors, with the gut microbiome playing a crucial role. The Crohn's disease-associated variant rs13107325 in the SLC39A8 gene results in an A391T substitution in the ZIP8 metal ion transporter and has previously been linked to alterations in the colonic microbiome in variant carriers. We hypothesized that the A391T substitution alters metal ion homeostasis in the colonic mucosal–luminal interface, thereby inducing dysbiosis which may promote intestinal inflammation.

Methods To evaluate this hypothesis, we generated a SLC39A8 A393T mouse model (matching human A391T). We first examined trace element abundance in the colonic mucosal epithelium and lumen of homozygous A393T and wild-type (WT) mice to determine if the variant affected metal distribution. We also performed 16S rRNA gene sequencing on colon samples at 2 months, 3–4 months, and 12 months of age, and conducted histological scoring of colon tissue collected from 5-month and 10-month old mice.

Results Consistent with an effect of the variant on ZIP8 function, homozygous A393T mice exhibited increased cobalt in the colonic mucosa, but reduced iron, zinc, manganese, cobalt, copper, and cadmium in the colonic lumen. 16S rRNA gene sequencing of colon samples revealed variant-linked effects on microbiome beta diversity in 2-month-, 3–4-month-, and 12-month-old mice. Histological scoring showed spontaneous intestinal inflammation in 10-month but not in 5-month-old mice. Lastly, predicted pathway analysis of the microbiome samples revealed differential enrichment of iron-, zinc-, and cobalt-dependent pathways in A393T mice compared to wild-type controls.

Conclusion These results suggest that the variant in SLC39A8 primarily restricts metal availability to the microbiota, resulting in compositions that can adapt to the environment and that A393T-linked dysbiosis occurs prior to the onset of inflammation. This study paves the way for future studies investigating risk variants as microbiome-disease modifiers.

✉ Jonathan P. Jacobs
jjacobs@mednet.ucla.edu

¹ The Vatche and Tamar Manoukian Division of Digestive Diseases, David Geffen School of Medicine at UCLA, Los Angeles, CA 90095, USA

² Icahn School of Medicine at Mount Sinai, New York, NY 10029, USA

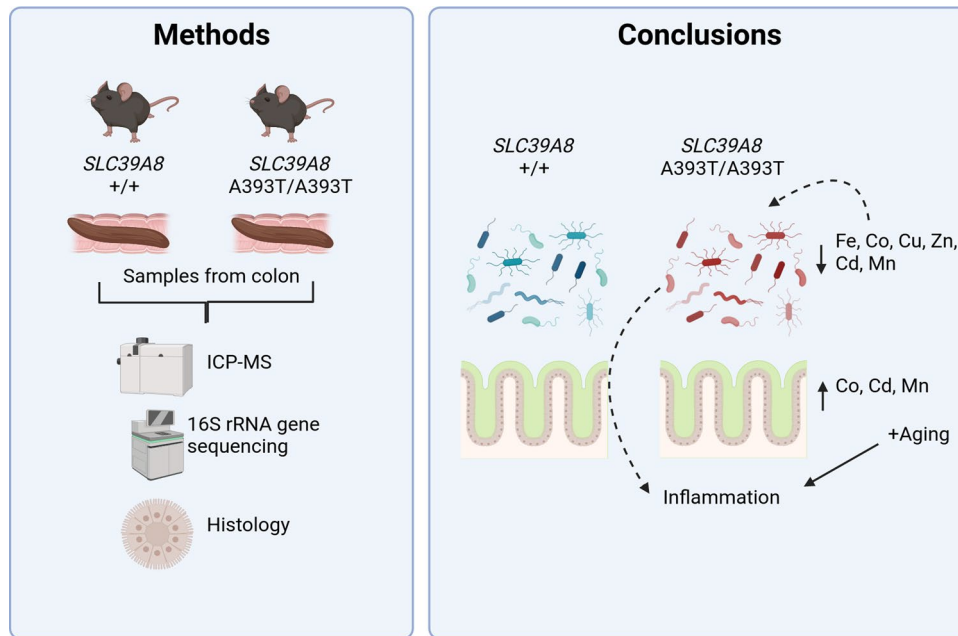
³ Department of Pediatrics, Division of Immunology, Allergy, and Rheumatology, David Geffen School of Medicine at UCLA, Los Angeles, CA 90073, USA

⁴ West China Hospital, Sichuan University, Chengdu, China

⁵ Division of Gastroenterology, Hepatology and Parenteral Nutrition, Veterans Affairs Greater Los Angeles Healthcare System, Los Angeles, CA 90073, USA

⁶ Goodman-Luskin Microbiome Center, UCLA, Los Angeles, CA 90095, USA

Graphical Abstract



Keywords Gene-environment · Microbiome · Crohn's disease · Mucosal-luminal interface · Trace metals

Introduction

Crohn's disease (CD) is an inflammatory bowel disease (IBD) characterized by inflammation along any part of the gastrointestinal tract, although it most commonly occurs in the ileocecal region. Both genetic and environmental influences are thought to contribute to the pathogenesis of Crohn's disease. CD-associated genetic risk factors have been reported through genome-wide association studies (GWAS); among these are variants in genes which regulate the immune response, such as *NOD2*, *CARD9*, and *REL*, and variants in genes which mediate tolerogenic responses to commensals, such as *IL10*, *IL27*, and *CREM* [1]. Lifestyle factors, such as smoking and diets high in saturated fat, have also been demonstrated to increase the risk of CD [2]. This has led to increasing attention to the possible involvement of the CD-associated gut microbiome as a vector of both genetic and environmental insults in mediating colitis. IBD risk variants, including *NOD2*, have been associated with altered gut microbiota composition in humans [3]. Therefore, interrogating whether CD risk variants can be disease-driving "microbiome quantitative trait loci" (mb-QTL) may be important to understanding the relationship between variant carrier status and heterogeneity in susceptibility to IBD [4].

Of the 200+ identified IBD risk variants from GWAS, the majority are non-coding, adding an additional layer of

difficulty for mechanistic research in preclinical models [5]. We and others have recently reported that the coding single-nucleotide polymorphism (SNP) rs13107325 in the gene *SLC39A8* resulting in the Ala391Thr substitution in the ZIP8 metal ion transporter is associated with Crohn's disease [6, 7]. We additionally reported that Thr allele carriage was associated with altered microbiome composition in mucosal lavage samples from both CD patients and their healthy controls, and microbes depleted in healthy control carriers overlapped with those depleted in CD patient carriers [6]. Since rs13107325 is also associated with other conditions spanning several organ systems, we hypothesized that this SNP may induce a diverse range of outcomes through its effects on the intestinal gut microbiome [8].

Two studies have since reported that A393T mice recapitulating the A391T human variant in *SLC39A8* exhibit increased intestinal inflammation in the dextran sulfate sodium (DSS) model of colitis. Both studies raised manganese tissue dyshomeostasis as a potential mechanism by which variant carrier status influences susceptibility to DSS-mediated colitis; however, conclusions on whether A393T carriers exhibit differential Mn abundance in the colon compared to their wild-type (WT) controls differed [7, 9]. These studies also did not address the impact of the variant on the colonic microbiome. Therefore, in this study, we sought to clarify the role of the *SLC39A8* variant on ZIP8 transport function at the colonic luminal–mucosal interface, on the

colonic microbiome, and on spontaneous and chemically induced inflammation and identify possible means by which these factors interact.

Materials and Methods

Construction of the SLC39A8 A393T Mouse Model

SLC39A8 A393T knock-in mice were created through fertilized C57Bl/6 oocyte injection of Cas9 DNA endonuclease, two guideRNA molecules [CTAGCTTTCGGCATT TTGGT] and [AGCGAGTGCAAATATAATAT] targeting the region encoding Ala393 in SLC39A8, and a single-stranded oligodeoxynucleotide donor template containing three point mutations corresponding to T393 in addition to silent mutations preventing further Cas9-mediated mutation (Figure S1). The injected, fertilized oocyte was then transferred into a pseudopregnant female. Sanger sequencing was used to validate successful gene knock-in of the offspring, which were subsequently backcrossed for three generations onto the C57Bl/6 background to mitigate the possibility of off-target gene editing. Wild-type, A393T/+, and A393T/A393T mice are respectively referred to as “WT”, “HET”, and “MUT” mice throughout this study.

Animals

Mice were given food (LabDiet 5053; irradiated) and water ad libitum and housed in static cages with autoclaved bedding under a 12:12 light:dark cycle. Colon samples were harvested from one cohort of 5-month-old mice for inductively coupled mass spectrometry and for histological scoring. For microbiomics sequencing, colonic luminal and mucosal samples were collected from one cohort of 2-month-old mice and one cohort of 12-month-old mice using a previously described protocol [15]. Fecal pellets from a separate cohort of 3–4-month-old mice were also collected and utilized for microbiomics sequencing. Mucus layer thickness was assessed in another cohort of 5–6-month-old mice. Two cohorts of mice aged 9–12 weeks were used for 2,4,6-Trinitrobenzene sulfonic acid (TNBS) or dextran sodium sulfate (DSS)-mediated chemical induction of colitis.

Mucus Layer Assessment

Mucus layer staining was performed using Alcian blue periodic acid-Schiff staining of paraffin-embedded, Carnoy's fixed colon tissue. Staining was performed using the Richard-Allan Scientific Alcian Blue pH 2.5 Periodic Acid-Schiff Stain Kit according to the manufacturer's protocol. Stained sections were assessed under light microscopy, and four images per animal were captured for mucus layer

measurement. Inner mucus layer thickness was assessed using the Java-based image-processing program ImageJ. After calibration with a hemocytometer grid, three measurements were taken per image, for a total of twelve measurements averaged per animal.

Histological Scoring

Hematoxylin and eosin-stained sections of colon were scored for the severity of intestinal inflammation as described by Erben et al. [16]. Scoring was performed by a single reviewer in a blinded manner. Histological scores ranged from 0 to 5, where 0 = none, 1 = minimal, 2 = mild, 3 = moderate, and 4/5 = marked. Scores were based on the observed level of inflammatory cell infiltration, epithelial changes, and mucosal architecture disruption. Inflammatory cell infiltration limited to the mucosa corresponded to an overall score of 1, any extent of submucosal infiltration corresponded to an overall score of 2–4, and transmural inflammation corresponded to an overall score of 5. Epithelial changes were assessed based on the level of epithelial hyperplasia, as well as the extent of goblet cell loss and presence of crypt abscesses. Mucosal architecture was assessed, in which the presence of crypt irregularity or loss, with or without ulcerations, corresponded to an overall score of 4–5.

Dextran Sodium Sulfate (DSS) Chemical Induction Model of Colitis

Mice were administered 2% DSS (MP Biomedicals cat # MFCD00081551) in drinking water for 7 days and switched to normal drinking water for 3 days. Body weights of the mice were obtained on the day prior to DSS administration and daily up to day 10 to calculate body weight as a percentage of baseline weight as the experiment's primary outcome. Following euthanization on day 10, colons were harvested and measured, since colon length shortening is an additional indicator of inflammation in the DSS model. [17]

Trace Element Assessment via Inductively Coupled Plasma Mass Spectrometry (ICP-MS)

To reduce the effects of recent intake on the intestinal ion concentrations, food and water were withheld from the mice for 4 h prior to euthanasia. Subsequently, the colon and the cecum were harvested. Luminal contents were collected via gentle squeezing of the intestines. Intestines were then cut lengthwise. One longitudinal half was cleaned in deionized water for ten seconds, which later became the “bulk colon tissue” samples for ICP-MS. The other longitudinal half was cleaned in phosphate-buffered saline (PBS) and then shaken vigorously in 15 mL of DMEM/1-mM dithiothreitol for 20 min at 37 °C. After shaking, an additional

15 mL of DMEM was added to the 50-mL conicals containing the samples and then the samples were vortexed and poured through a 70- μ M filter. The samples were then centrifuged at 2000 \times g for 20 min, decanted, re-suspended in 15-mL DMEM, centrifuged at 2000 \times g for 20 min, and then decanted. The pellets were then re-suspended in 15-mL PBS, centrifuged at 700 \times g for 8 min at 4 °C, then decanted, re-suspended in 2-mL PBS, transferred to an Eppendorf tube, and then centrifuged for the last time at 700 \times g for 8 min. Remaining PBS was removed with a pipette, taking care not to disturb the pellet. All centrifugation was performed at 4 °C. The colonic luminal, cleaned colon tissue, and mucosal epithelial cell pellets were then dried at 60 °C for 16 h to obtain the dry weight. ICP-MS (NexION 2000, PerkinElmer) analysis was performed to detect multiple elements (Fe, Co, Cu, Zn, Cd, Mn) in the samples. All samples were used as received without further purification or modification. Each sample was transferred to a clean Teflon vessel for acid digestion. Digestion was carried out with concentrated HNO₃ (65–70%, Trace Metal Grade, Fisher Scientific) with a supplement of H₂O₂ (30%, Certified ACS, Fisher Scientific) at 190 °C for 20 min in a microwave digestion system (Titan MPS, PerkinElmer). Once the sample was cooled to room temperature, it was subsequently diluted to make a final volume of 50 mL by adding filtered deionized water for analysis. The calibration curve was established using a standard solution, while the dwell time was 50 ms with thirty sweeps and three replicates with background correction.

2,4,6-Trinitrobenzene Sulfonic Acid (TNBS) Chemical Induction Model of Colitis

This protocol was adapted from Wirtz et al. [18]. Briefly, mice were pre-sensitized one week prior to intrarectal administration with 2.5% TNBS. For pre-sensitization, a 1% TNBS solution was applied to a shaved 1.5 \times 1.5 cm spot on the backs of the mice. After 7 days, 2.5% TNBS in ethanol was administered intrarectally with a rubber-tipped needle into anesthetized mice. The mice were held by the tail, snout downward, for an additional minute to ensure proper administration. Mice were weighed for 3 days afterward, and the lengths of colons were measured following euthanasia.

16S rRNA v4 Gene Sequencing

DNA was extracted from the colonic luminal content of 2-month-old mice and 1-year-old mice utilizing the Zymo-biomics DNA Miniprep Kit (cat#D4300) according to the manufacturer's protocol. For fecal pellet samples from 3 to 4-month-old mice, DNA extractions were performed with the Qiagen DNeasy PowerSoil Pro Kit (cat#47014). Next, to amplify the v4 region of the 16S rRNA gene,

polymerase chain reactions (PCR) were setup for each sample using the extracted DNA as the template and primers 515F and 806R as previously described [19]. PCR products were then purified with the ZR-96 DNA Clean & Concentrator-5 (cat#D4024) kit and pooled together for paired-end sequencing with Illumina NovaSeq. Following quality filtering and merging of raw reads utilizing the DADA2 package in R, a count table of unique amplicon sequence variants (ASV) \times samples was obtained for each cohort (2 months, 3–4 months, and 1 year old). Taxonomy assignment of the ASVs was achieved using the naive Bayes classifier trained on the Silva 138.1 database. For the 2-month and 1-year cohorts, the datasets were stratified by sample type (Luminal or Mucosal) prior to further analysis. The 2-month-old mice were sequenced in two batches (encoded by the variable Sequencing_Run). The 2-month-old and 1-year-old cohorts included luminal and mucosal samples collected from the cecum, proximal colon, and distal colon (encoded by the variable Site), whereas the 3–4-month-old samples were sequenced in one batch with one fecal sample per mouse. Square-root Jensen–Shannon dissimilarity matrices were calculated on the ASV count tables prevalence filtered to 15% and were then visualized by principal coordinates analysis. Repeated measures PERMANOVA on the dissimilarity matrix was used to determine the effect of Genotype, after accounting for Sex (for the 3–4-month-old mice), or after accounting for Site and Sex (for the 1-year-old mice), or after accounting for Sequencing_Run, Site, and Sex (for the 2–3-month-old cohort). For differential taxon association testing, ASV counts were first collapsed to the genus level. Next, the log-transformed, total sum scaling-normalized, and 15% prevalence filtered genus-level counts were fitted to linear mixed-effects models (LMEM) implemented in MaAsLin2, with Sex and Genotype as fixed effects (3–4 months), Site, Sex, and Genotype as fixed effects and MouseID as a random effect (1 year), and Sequencing_Run, Site, Sex, and Genotype as fixed effects with MouseID as a random effect (2 months) [20]. A genus was considered as significantly differentially abundant if the *q*-value (false discovery rate-corrected *p*-value) was less than 0.25. The PICRUSt2 algorithm was used to generate predicted pathway abundances based on the 16S data [14]. Subsequently, the same LMEMs were fitted to the pathway abundance data in order to identify pathways differentially enriched in MUT compared to WT mice following multiple hypothesis correction (*q* < 0.25). Circle plots grouping enriched pathways into higher-order hierarchies defined by MetaCyc were generated with package “circlize” in R. Analysis scripts and input files sufficient to replicate the figures (with the exception of Fig. 1) are publicly available on <https://github.com/jacobslabucla/slccolon/>.

Results

SLC39A8 Variant Affects Predicted ZIP8 Structure and Disrupts Trace Element Homeostasis in the Colon

Given that the SNP rs13107325 results in the substitution of the nonpolar Ala residue to the polar Thr residue, we reasoned that this could affect the ZIP8 protein structure and lead to functional effects on ion transport. Since the structure of ZIP8 has not yet been determined experimentally, we utilized the AlphaFold2 structural prediction algorithm to generate and overlay the predicted structures of human ZIP8 A391 and ZIP8 T391 [10]. Although the distance between Ala and Thr at the 391 position was only 1.35 Å as measured between alpha carbons, key glutamine and histidine residues which are purported to mediate metal ion binding in ZIP transporters were shifted by 3.49 and 3.83 Å in the structural overlay (Fig. 1) [11].

To evaluate whether the changes in ZIP8 structure were accompanied by changes in function, we generated ZIP8 A393T mice recapitulating the human variant by CRISPR-Cas-mediated gene editing followed by three rounds of backcrossing. We then examined trace element abundance in colonic luminal, mucosal, and cleaned bulk tissue samples collected from wild-type (WT) mice and homozygous (MUT) A393T mice with inductively coupled plasma mass spectrometry (ICP-MS). Trace elements evaluated included

iron, cobalt, copper, zinc, cadmium, and manganese (Fig. 2). Compared to WT mice, MUT mice exhibited significantly lower levels of the above elements in the colonic luminal samples, higher cobalt abundance in the mucosal epithelium, and higher cobalt, cadmium, and manganese in the cleaned bulk tissue ($p < 0.05$ for all elements) (Fig. 2). These results suggest that the functional consequences of ZIP8 A391T include increased uptake of these dietary elements by the host and conversely, reduced bioavailability of these elements for the intestinal microbiota.

SLC39A8 Variant Induces Microbiome Compositional and Predictive Functional Shifts that Increase with Age

Iron, copper, zinc, and manganese are critical to the survival and fitness of many bacterial organisms, while cobalt and cadmium exposure have been reported to affect the gut microbiome [12, 13]. Since we observed ~25% reduction in all of these trace elements in the luminal samples of MUT compared to WT mice, we hypothesized that this would affect the gut microbiome of variant carriers. To thoroughly evaluate effects of the variant on the gut microbiome, we performed 16S rRNA gene sequencing of samples collected from three cohorts of mice: colonic luminal and mucosal-adherent microbiota of 2-month- and 12-month-old WT, heterozygous (HET), and MUT mice, along with the fecal microbiota of 3–4-month-old WT, HET, and MUT mice.

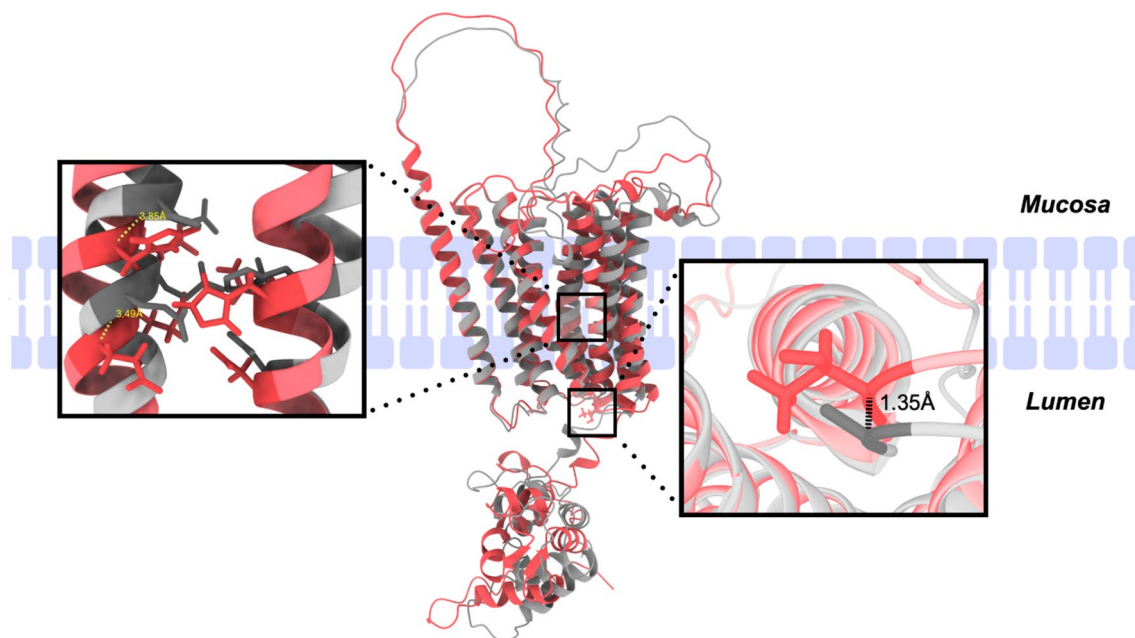


Fig. 1 Overlay of ZIP8 A391- and ZIP8 T391-predicted structures. ZIP8 A391 (gray) and ZIP8 T391 (red) structures were generated with the AlphaFold2 structural prediction algorithm and overlaid in UCSF ChimeraX. The right box highlights the distance between

alpha carbons in the residues at the 391 position. The left box highlights an EEXXHE motif on transmembrane domain V and HNXXD motif on transmembrane domain IV

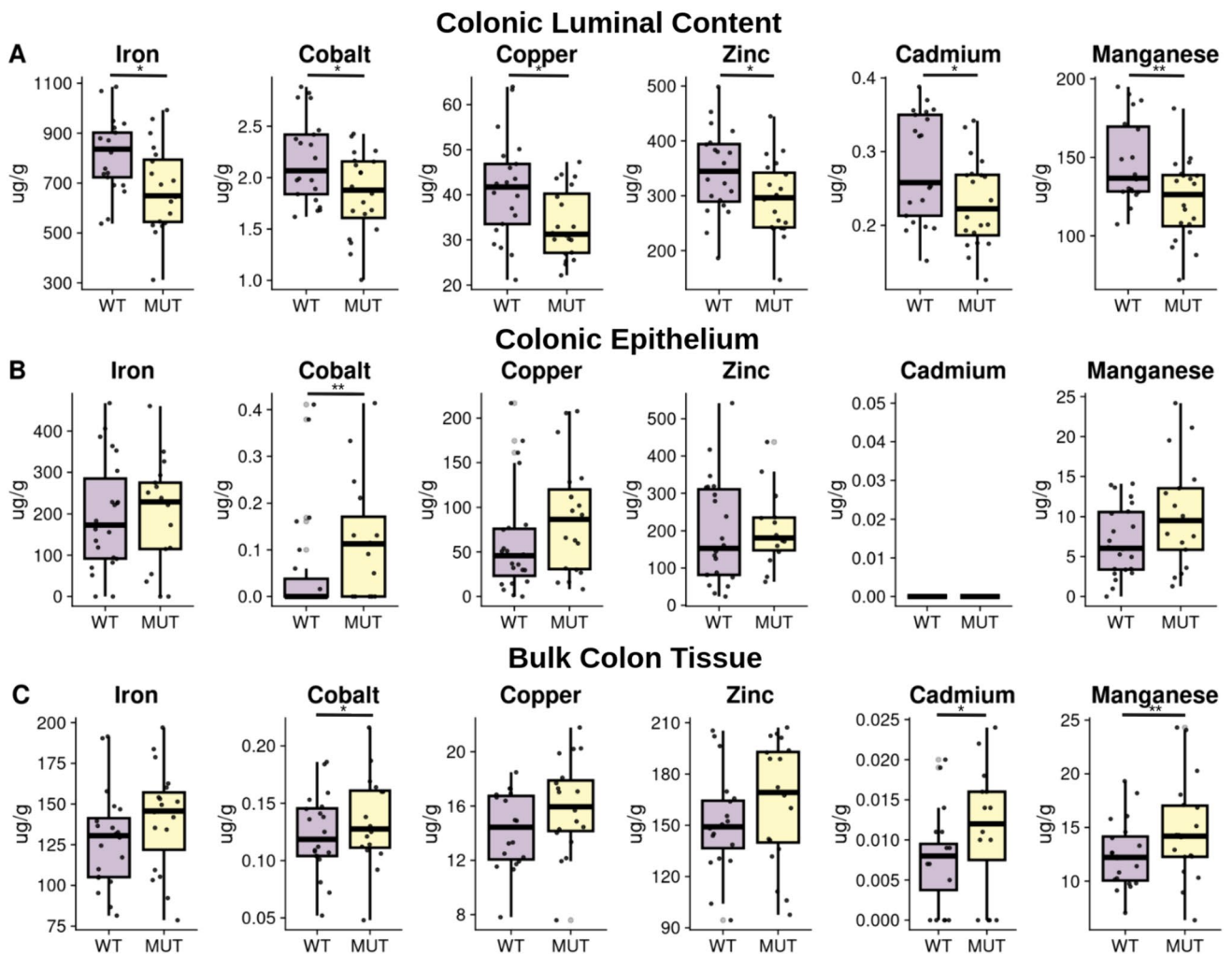


Fig. 2 MUT mice exhibit altered luminal:mucosal trace element distributions compared to their WT counterparts. Harvested samples from 5-month-old WT ($n=13$ females (F) and $n=12$ males (M)) and MUT ($n=12$ F and 11 M) mice were utilized for trace element analysis via inductively coupled plasma mass spectrometry (ICP-MS). Box plots show the distributions of trace element abundance by genotype

in units of $\mu\text{g/g}$ dry weight for colonic luminal content (A), colonic mucosa (epithelial cells) (B), and bulk colon tissue (C), with outliers removed according to the 1.5 Interquartile Range criteria for visualization purposes only. Statistical analysis was performed on the whole dataset using Wilcoxon rank-sum tests comparing WT to MUT; * $p < 0.05$; ** $p < 0.01$

Due to the feces being representative of the contents in the distal end of the colon, we compared the 3–4-month cohort to the 2- and 12-month colonic luminal samples.

In the 2-, 3–4-, and 12-month-old luminal/fecal content, relative abundances of highly abundant bacteria were similar among the WT, HET, and MUT mice (Fig. 3A–E). However, visualization of microbiome beta diversity through principal coordinates analysis (PCoA) of Jensen–Shannon distances illustrates MUT sample clustering along the PC1 axis (Fig. 3F, H, J). In all three luminal/fecal cohorts, PERMANOVA of the Jensen–Shannon distance matrix revealed that genotype (encoding WT, HET, or MUT) was significantly associated with microbiome composition, with R^2 (effect size) values increasing from 3% in the 2-month cohort to 9% in the 12-month cohort (Fig. 3F, H, J).

Similarly, the 2- and 12-month-old colonic mucosal samples did not show differences in highly abundant bacteria among the WT, HET, and MUT mice in the taxonomic summary plots, with the exception of reduced relative abundance in *Pseudomonas* of HET and MUT compared to WT 2-month-old colonic mucosa and reduction in *Ligilactobacillus* in MUT compared to WT 12-month-old colonic lumen and mucosa (Fig. 3B, 3D). While differences in mucosal colon community structure by genotype were only marginally significant for the 2-month-old mice, the association of genotype with gut microbiome was statistically significant with an R^2 of 6% in the 12-month-old mice (Fig. 3I). There were no differences in microbiome alpha diversity as assessed through the Shannon index (species richness and evenness) or by total number of amplicon sequence variants

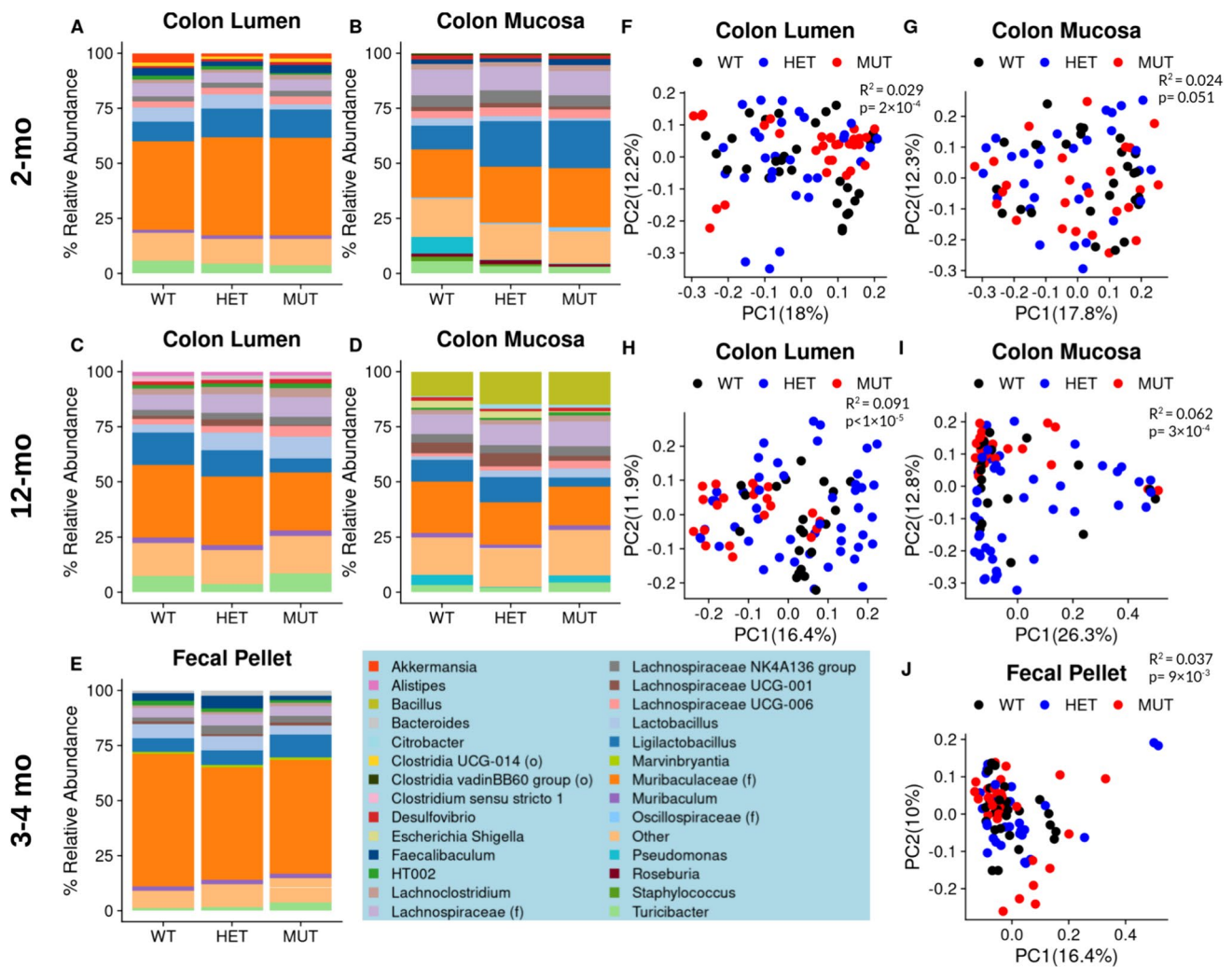


Fig. 3 MUT mice exhibit a distinct microbiome composition in three differently aged cohorts. Taxonomic column summary plots illustrate the % relative abundance of genera which comprise at least 1% of the microbiome composition in the colonic lumen or adhered to the colonic mucosa of 2-month-old WT, HET, and MUT mice (A, B), 12-month-old mice (C, D), or the fecal pellets of 3–4-month-old mice (E). The genera color legend for all barplots is shown at the bottom of the figure. If the name of the genus is unknown, its family name (f) or order name (o) is shown. Principal coordinates analysis plots on square-root Jensen–Shannon dissimilarities illustrate the differences

in microbiome composition between WT, HET, and MUT mice, with each dot representing one sample. Plots are shown for the colonic lumen or colonic mucosa of 2-month-old (F, G), 12-month-old (H, I), or the feces of 3–4-month-old (J) mice. R^2 and p -values associated with the effect of Genotype are reported from PERMANOVA of sample dissimilarity matrices. The microbiome data represents $n = 10$ WT (4 F 6 M), $n = 10$ HET (4 F 6 M), and $n = 10$ MUT (4 F 6 M) for 2-month-old mice and $n = 27$ WT (11 F 16 M), $n = 30$ HET (10 F 20 M), and $n = 31$ MUT (14 F 17 M) for 3–4-month-old mice

(ASVs) across genotypes for any of the datasets with the exception of increased ASVs in MUT compared to WT colonic mucosal samples (Figure S2). Overall, these findings support an effect of variant carrier status on microbiome beta diversity which increases with age and is greater in the luminal compartment of the colon than in the mucosal-adherent fraction.

Next, to assess whether changes in the abundance of specific genera accompany the MUT-linked differences in microbiome composition, we performed differential genera abundance testing comparing MUT to WT mice.

While only 5–7 differentially abundant genera were found in the 2- and 3–4-month-old mice, 18 and 29 differentially abundant genera were found in the 12-month-old mice (Fig. 4). Most differentially abundant genera had a relative abundance of < 1%, with the exception of *Lactobacillus* and *Ligilactobacillus* in the 2- and 12-month-old mice, respectively, and genera belonging to *Muribaculaceae* in the 3–4-month-old mice (Fig. 4A–D). Compared to their WT counterparts, *Lactobacillus* was significantly reduced in the 2-month-old MUT mice in the colonic lumen, *Ligilactobacillus* was decreased in the luminal and mucosal colons of

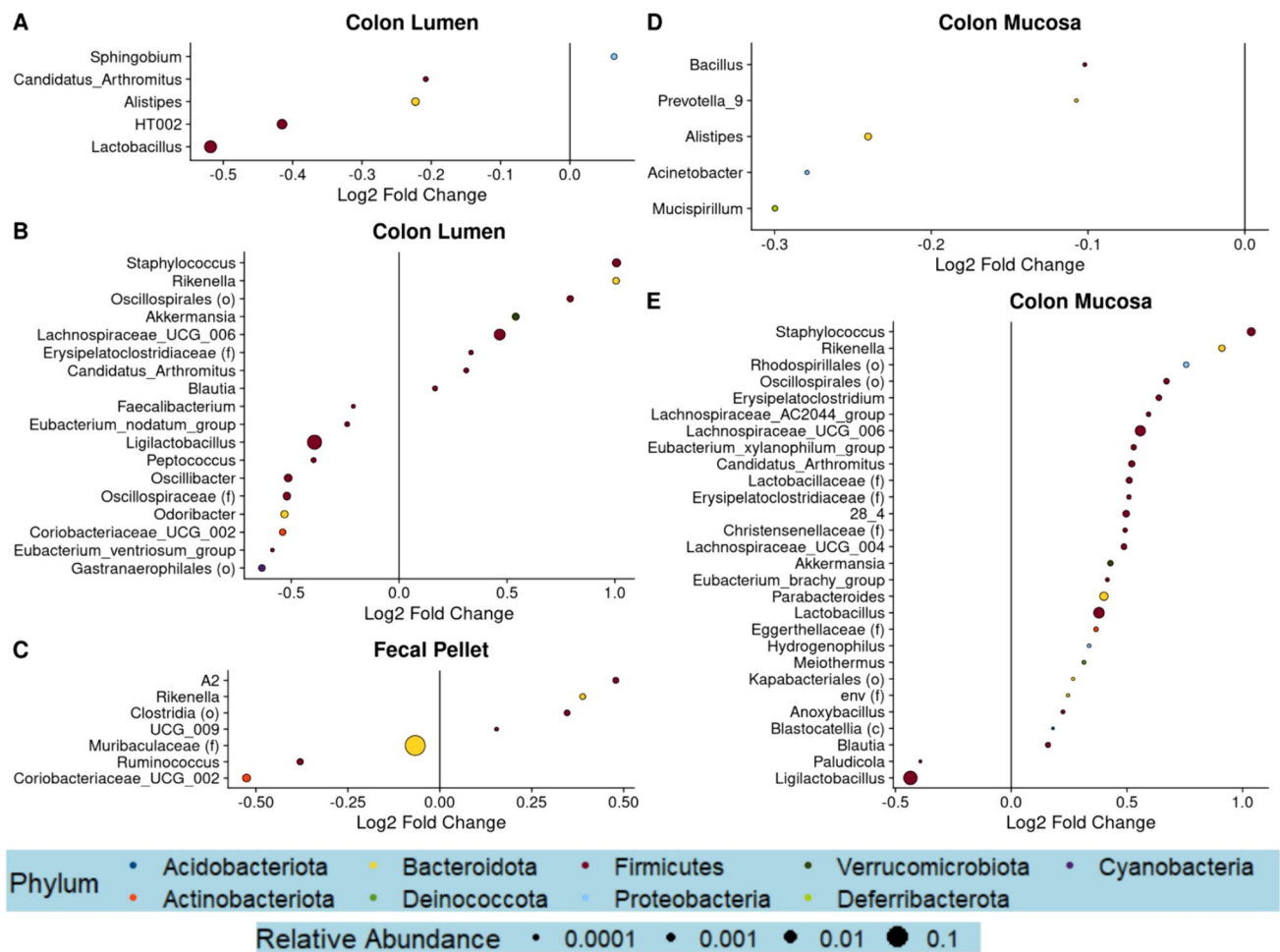


Fig. 4 MUT mice exhibit altered abundance of several genera compared to WT mice. Differential abundance testing was performed at the genus level utilizing linear mixed-effects models of log-transformed, normalized count data. Dot plots visualizing significantly differentially abundant genera (false discovery rate-adjusted p -value,

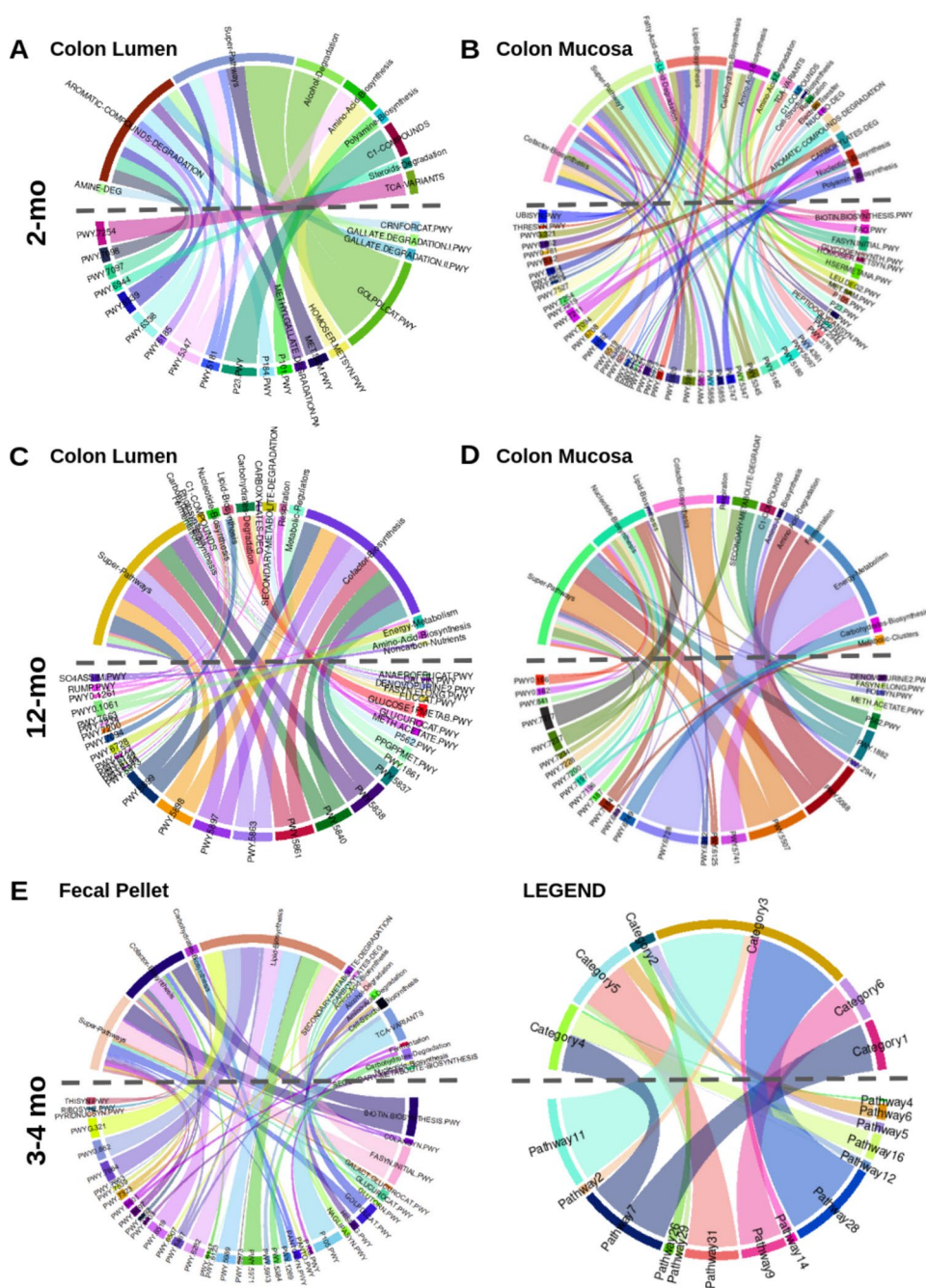
$q < 0.25$) between MUT and WT are shown for the colonic lumen or colonic mucosa datasets of the 2-month-old mice (**A**, **D**), the 12-month-old mice (**B**, **E**), or the fecal pellets of the 3–4-month-old mice (**C**). The size of the dot corresponds to the relative abundance of the genera, while the color of the dot represents the phylum

the 12-month-old MUT mice (Fig. 4B, D), and Muribaculaceae was significantly reduced in the 3–4-month-old MUT mice (Fig. 4A–D). Interestingly, *Staphylococcus*, *Rikenella*, *Akkermansia*, and *Candidatus_Arthomitus* were among 7 shared genera which were enriched in MUT compared to WT mice between both luminal and mucosal compartments of 12-month-old mice, while no such overlap was observed in 2-month-old mice (Fig. 4A–D). Notably, across the three cohorts of mice, no genera were found to be differentially abundant in the same direction. These results suggest that variant-linked perturbations in microbiome community increase with age and may be due to broad shifts in multiple low-abundance bacterial taxa, rather than differential abundance of any particular bacteria.

Since we did not identify genera which were consistently linked to variant carrier status across the three cohorts of mice, we investigated whether there were consistent patterns in

microbial function that would better characterize the effects of the variant on the microbiome. To accomplish this, we utilized the PICRUSt2 pipeline to predict MetaCyc pathway abundances from the 16S rRNA gene sequencing count data [14]. Predicted functional pathways which were identified as being significantly differentially enriched were present in all three cohorts. To identify patterns among the differentially enriched pathways, we grouped each individual pathway (bottom half of circular map) into higher-order classifications (top half of maps) (Fig. 5). Interestingly, pathways classified as “cofactor biosynthesis” were observed in five out of six datasets, with the exception of the colonic lumen dataset in 2-month-old mice (Fig. 5; Table S1). In 2-month-old mice, all 10 differentially abundant pathways classified as “cofactor biosynthesis” were depleted among mucosal-adherent bacteria of MUT mice compared to WT mice (Fig. 5B; Table S2). In the 3–4-month-old cohort, pathways classified as “cofactor biosynthesis” were

Fig. 5 MUT mice exhibit differential abundance of predicted functional pathways. The PICRUST2 algorithm was used to generate predicted MetaCyc pathway abundances from the 16S rRNA gene compositional data. Genotype-associated pathways were identified through linear mixed-effects regression. Circle plots group pathways which significantly distinguished ($q < 0.25$) MUT from WT mice into higher-order categories, for the colonic luminal and colonic mucosal datasets of 2-month-old (A, B) or 12-month-old mice (C, D), or the fecal pellets of 3–4-month-old mice (E). The pathways are identified by their MetaCyc pathway IDs on the bottom half of the circle plots, while the higher-order categories are identified by name on the top half of the circle plots. One pathway can belong to multiple categories; in the legend, Pathway 7 maps to both Categories 1 and 4. The color of each chord corresponds to the pathway, while the width of the chord corresponds to the absolute value of the regression coefficient or effect size (the larger the effect of genotype on the pathway, the wider the chord; in the legend, the effect of genotype of Pathway 28 is large, while the effect of genotype on Pathway 2 is small)



both depleted and enriched, while in 12-month-old mice, all 8 and 5 “cofactor biosynthesis” pathways in the colonic lumen and mucosa samples were exclusively enriched in MUT compared to WT mice (Fig. 5C–E; Tables S3–S5).

SLC39A8 Variant Mediates Spontaneous Colonic Inflammation but Does Not Modulate Susceptibility to Chemically Induced Colitis

To evaluate whether MUT mice exhibit intestinal inflammation in a manner consistent with the Crohn’s disease risk

conferred by SLC39A8 A391T variant carriage in humans, we performed histological scoring of hematoxylin and eosin-stained colon tissue from 5-month-old to 10-month-old mice. There were no differences in inflammation between 5-month-old MUT and WT mice (Fig. 6A, B). Additionally, in contrast to what was previously reported, there were no differences in mucus barrier thickness as assessed through Alcian Blue/Periodic Acid-Schiff staining between 6-month-old MUT and WT mice (Supplemental Fig. 2) [9]. However, increased inflammation was observed in 10-month old MUT compared to WT mice (Fig. 6C–D). This suggests that

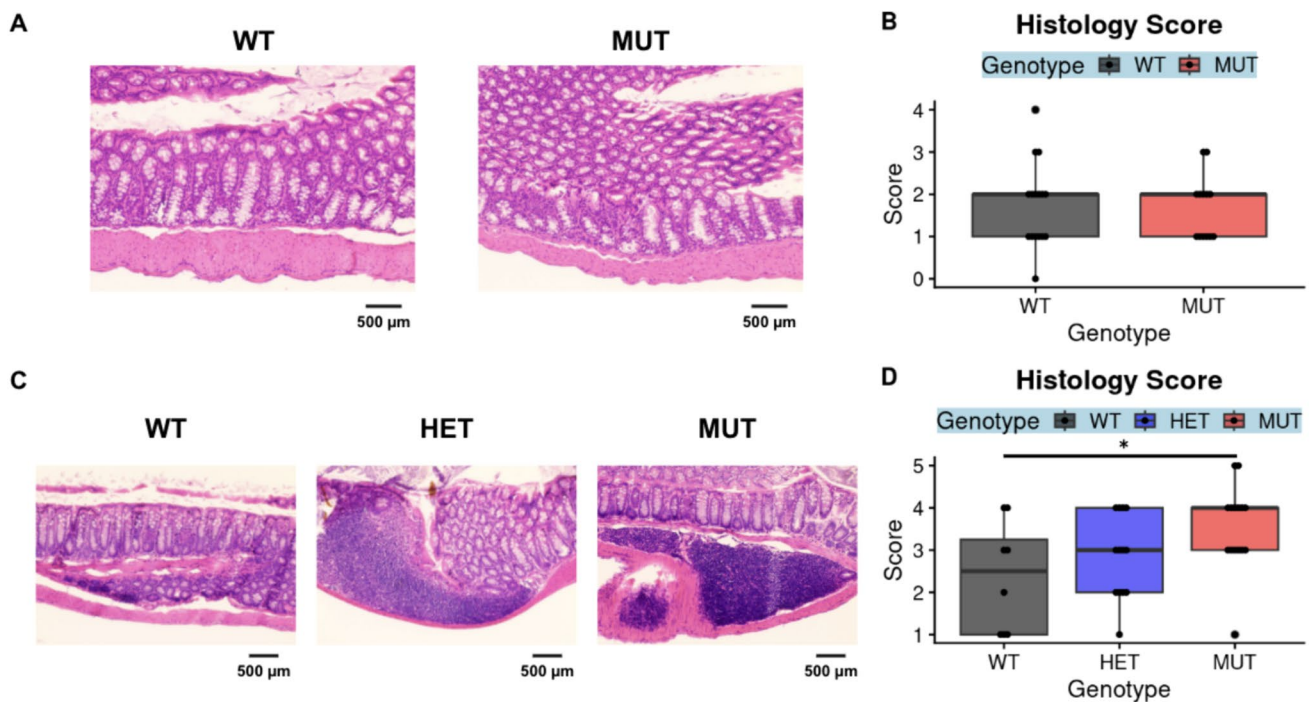


Fig. 6 MUT mice exhibit age-dependent changes in spontaneous inflammations. Formalin-fixed, paraffin-embedded sections of colon tissue were stained with hematoxylin and eosin and scored for inflammation as assessed by lymphocyte infiltration and tissue architecture. Images and scores from colons from 5-month-old mice (the ICP-MS cohort) are shown in **A, B**, and images and scores from colons from 10-month-old mice are shown in **C, D**. Representative images were

obtained through brightfield microscopy at 20× magnification (**A, C**) with a scale bar representing 500 microns. Significance was assessed through Wilcoxon rank-sum tests comparing WT to HET or WT to MUT, * $p < 0.05$. The data in **A, B** represent 16 WT (7 F 9 M) and 13 MUT (4 F 9 M) mice, where the data in **C, D** represent $n = 12$ WT (6 F 6 M), $n = 11$ HET (5 F 6 M), and $n = 11$ MUT (7 F 4 M) mice

inflammation due to carriage of the Thr allele spontaneously develops, but may require an additional insult, such as aging.

Two other studies have reported increased susceptibility of MUT compared to WT mice to dextran sodium sulfate (DSS)-induced colitis (one cohort aged 9–12 weeks, the other 11.5–13 weeks) [7, 9]. We sought to reproduce these results by administering DSS to 9–12-week-old WT, HET, and MUT mice to induce colitis. Mice were compared on three primary outcomes: body weight as a percent of baseline body weight prior to induction (where % baseline body weight decreases with increasing disease severity), colon length (where colon length is inversely related to inflammation), and colon histology score (where greater scores indicate higher disease severity) (Fig. 7). Hematoxylin and eosin-stained colons from the DSS-treated cohort additionally underwent histological scoring. There were no differences by genotype in body weight, colon length, or histological scores for DSS-treated mice (Fig. 7A-D). To confirm the absence of vulnerability to chemically induced colitis, we additionally utilized a second model—the 2,4,6-Trinitrobenzene sulfonic acid (TNBS) model. There were no differences by genotype in body weight or in colon length in the TNBS-treated mice (Fig. 7E-F).

Discussion

The relationship between genetic risk, the human gut microbiome, and IBD is unclear but remains critical to enhancing predictions of disease risk and developing more personalized therapies. Emerging evidence from GWAS, including those with microbial abundances as quantitative traits [21], and microbiota studies in gene knockout preclinical models supports the notion that SNPs in susceptibility genes may confer disease risk through modulation of the microbiota [22, 23]. Despite this, few studies have investigated the impact of specific risk loci on gut microbiome composition, aside from the Atg16L1 T300A variant [24]. We report here, for the first time, that the Crohn’s disease linked missense variant in SLC39A8 modulates colonic microbiome composition, consistent with what has previously been reported in human Crohn’s disease patients and in healthy control variant carriers [6]. These results position SLC39A8 A391T as a possible Crohn’s disease-driving microbiome quantitative trait locus (mb-QTL).

Utilizing multiple cohorts of SLC39A8 A393T (matching human A391T) mice in this study, we demonstrated that the effects of A393T on microbiome community structure

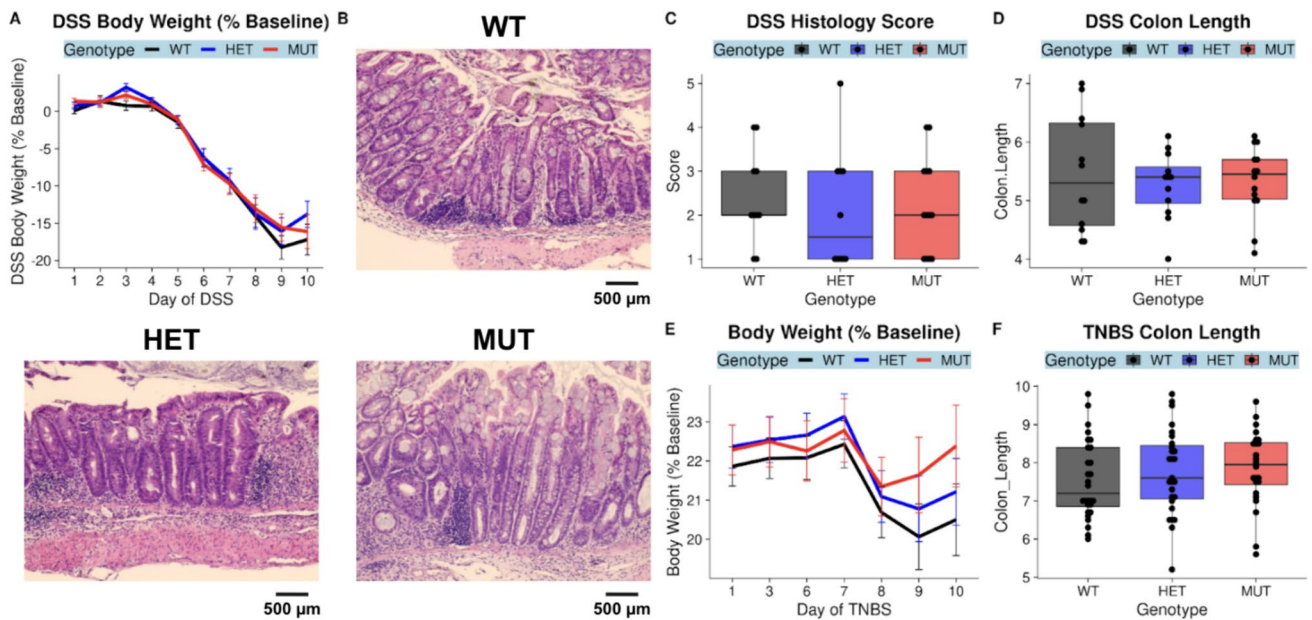


Fig. 7 The A393T variant does not increase susceptibility to DSS- or TNBS-mediated chemical induction of colitis. DSS was administered via the drinking water to 2–3-month-old mice, and body weight loss assessed as % of baseline was tracked for 10 days (A). Formalin-fixed, paraffin-embedded colon tissue sections were stained with hematoxylin and eosin and scored for inflammation. Representative colon images by genotype are shown in B, and the distribution of histology scores by genotype are shown in C. Differences in colon length (cm) by genotype are shown in D. The DSS cohort represents $n = 13$ WT mice (4 F 9 M), $n = 13$ HET (4 F 9 M), and $n = 15$ MUT (3

F 12 M) mice. In another cohort of 2–3-month-old TNBS mice, mice were pre-sensitized on Day 0 and injected intrarectally with TNBS on Day 7. Body weight loss assessed as % of baseline was tracked for 3 days following the injection (E). Distributions of colon length (cm) by genotype for TNBS mice are shown in F. Representative images were obtained through brightfield microscopy at 20 \times magnification (B) with a scale bar representing 500 microns. The TNBS cohort was composed of $n = 20$ WT (8 F 12 M), $n = 22$ HET (8 F 14 M), and $n = 17$ MUT (5 F 12 M) mice

were apparent in 2-month-old, 3–4-month-old, and 1-year-old mice. We additionally identified intestinal inflammation through histological analysis in 10-month-old mice but not 5-month-old mice. Although our study was not truly longitudinal, we can leverage this cross-sectional data from mice at different ages to conclude that A393T-linked microbiome dysbiosis occurs prior to the onset of intestinal inflammation. This supports the idea that risk variant carriage regulates the microbiome as a step in pathogenesis. These findings also mirror observations in a longitudinal study of Crohn’s disease patients, where higher instability in the gut microbiome in the remission phase was associated with higher risk of flare [25].

To better understand this A393T-linked microbiome signature on overall community structure, we performed differential taxon abundance testing and differential predicted pathway enrichment analysis in MUT compared to WT mice. While there were no concordant A393T-linked genera across different age cohorts, pathways mapping to “cofactor biosynthesis” were consistently differentially enriched in MUT compared to WT mice. Divalent cations transported by ZIP8, including iron, zinc, manganese, copper, and cobalt are utilized by members of the gut microbiome for processes including antioxidant response and metabolism [13,

26]. These metal ions often serve as cofactors for enzymes involved in these processes, such as iron for heme [27]. Increased exposure to several of these metals or metal-deficient diets have been shown to affect the composition of the gut microbiome [28–31]. At the colonic mucosal–luminal interface, we found that MUT mice exhibited reductions of iron, zinc, manganese, copper, cobalt, and cadmium in the lumen and increased abundance of specifically cobalt in the epithelial cells. Several of the predicted cofactor biosynthesis pathways differentially enriched in MUT mice employ metal-dependent enzymes. These included depletion of iron-dependent heme biosynthesis among mucosal-adherent bacteria of 2-month-old mice, depletion of zinc-dependent folate biosynthesis in the feces of 3–4-month-old mice, and enrichment of two cobalt pathways (cob(II)yrinate a,c-diamide biosynthesis I and adenosylcobalamin biosynthesis I) in the mucosal-adherent bacteria of 1-year-old mice [32]. Although the direction in which these predicted pathways are differentially enriched do not appear to concur with the trace element abundance results from ICP-MS, under conditions of metal depletion, some bacteria may have strategies to employ alternative metal-independent enzymes in critical processes [32]. Thus, microbiome dysbiosis in MUT mice may be secondary to the metal dyshomeostasis in these

mice. Future studies that include metatranscriptomics could provide further insight into bacterial responses to altered trace metal availability in MUT mice.

There were several notable differences between our findings and those of prior studies of SLC39A8 A393T mice. Consistent with a loss-of-function conferred by the variant, previous ICP-MS of A393T mice revealed that MUT compared to WT mice exhibited reduced Mn in blood and liver tissues [7, 9]. However, while Sunuwar et al. found no differences in trace element abundance in the colons of MUT and WT mice aged 9–14 weeks of age, Nakata et al. reported 30–32-week-old MUT mice exhibited reduced Mn abundance in MUT compared to WT colons. In bulk colon tissue, we actually found increased Mn abundance in MUT compared to WT colons. Our findings in 17–22-week-old mice suggest that the consequences of the ZIP8 substitution at the apical surface of the colon is a gain of function, whereas in MUT mice there is increased uptake of several metals while restricting the pool of available ions in the lumen. One possibility is that this discrepancy may be due to study-specific designs (e.g., age and sex) as well as experimental variability across studies with small sample size. Another possibility is that this is a physiologically relevant outcome related to microbiome differences across facilities, revealing both strengths and weaknesses of performing these gene-microbiome studies. If the risk variant indeed confers disease susceptibility through its effects on the microbiome (which is additionally affected by environmental exposure), there is also the possibility that the microbes and microbe-derived signals affect the expression of other genes [22]. With our facility-specific microbiome, this may manifest itself as upregulation of redundant transporters for Zn, Mn, and Fe, such as ZIP14, that compensate for reduced uptake by ZIP8 [33]. Supporting this notion, Nakata et al. and Sunuwar et al. reported increased susceptibility to DSS-induced colitis in MUT compared to WT mice, while we did not observe any differences between the two. Nakata et al. also reported thinner mucus layers in MUT mice compared to WT mice that they proposed was due to a reduction in Mn-dependent glycosylases, but we did not observe a difference between MUT and WT mice. The importance of microbiome differences across facilities in the outcome of DSS colitis experiments has recently been demonstrated by Forster et al., who reported that susceptibility to DSS-induced colitis varied across facilities in a manner that depended on whether specific microbes were present within the microbiota of each facility [34].

In summary, we found that the SLC39A8 variant affects colonic mucosal–luminal trace metal homeostasis, changes the microbiome prior to disease onset, and promotes eventual spontaneous colitis representing a model for how it could promote disease in humans. Future SLC39A8 variant-associated microbiome transfer studies (from human and/or mouse variant carriers) will be critical to understanding

whether the genetic risk-associated microbiome can indeed drive intestinal inflammation. Our study highlights the potential for other IBD-associated genetic risk variants to follow a similar paradigm in which the microbiome is altered as an intermediate step to the development of intestinal inflammation.

Supplementary Information The online version contains supplementary material available at <https://doi.org/10.1007/s10620-024-08647-8>.

Acknowledgments The authors acknowledge the use of the ICP-MS facility within the UC Center for Environmental Implications of Nanotechnology in CNSI at UCLA, the Microbiome Core of the Goodman-Luskin Microbiome Center for performing microbiome sequencing, the UC Irvine Transgenic Mouse Facility for generation of the SLC38 A393T mice, and the Translational Pathology Core Laboratory for embedding, sectioning, and performing the hematoxylin and eosin-staining of the intestines. The authors additionally acknowledge the use of BioRender.com in preparing the graphical abstract.

Author's contribution Conceptualization: J.P.J. Data curation: J.C.Y. Formal analysis: J.C.Y. (Lead) and M.Z. (Supporting) Funding acquisition: J.P.J. and D.C. Investigation: N.A.J., Z.Y., J.C.Y., (Lead) M.Z., D.C., J.S., A.G., C.C., F.L., and V.L. (Supporting) Methodology: J.P.J., J.C.Y., V.L., N.A.J., and Z.Y. Project administration: J.C.Y., N.A.J., Z.Y., and V.L. Resources: J.P.J. and V.L. Software: J.C.Y. Supervision: J.P.J., J.C.Y., N.A.J., and Z.Y. Validation: M.Z. Visualization: J.C.Y. and M.Z. Writing—original draft: J.C.Y. (Lead), M.Z., and D.C. (Supporting) Writing—review & editing: J.P.J.

Funding The research is supported by the Vatche and Tamar Manoukian Division of Digestive Diseases and the UCLA Children's Discovery and Innovation Institute (CDI) Fellows Research Support Award. J.P.J. was supported by VA CDA2 IK2CX001717.

Data availability Raw sequencing data is available on NCBI Bioproject via the accession code PRJNA1004665.

Declarations

Conflict of interest All authors confirmed they have no disclosures to make.

Open Access This article is licensed under a Creative Commons Attribution 4.0 International License, which permits use, sharing, adaptation, distribution and reproduction in any medium or format, as long as you give appropriate credit to the original author(s) and the source, provide a link to the Creative Commons licence, and indicate if changes were made. The images or other third party material in this article are included in the article's Creative Commons licence, unless indicated otherwise in a credit line to the material. If material is not included in the article's Creative Commons licence and your intended use is not permitted by statutory regulation or exceeds the permitted use, you will need to obtain permission directly from the copyright holder. To view a copy of this licence, visit <http://creativecommons.org/licenses/by/4.0/>.

References

1. Khor B, Gardet A, Xavier RJ. Genetics and pathogenesis of inflammatory bowel disease. *Nature*. 2011;474:307–317. <https://doi.org/10.1038/nature10209>.

2. Dam AN, Berg AM, Farraye FA. Environmental influences on the onset and clinical course of Crohn's disease—part 1: an overview of external risk factors. *Gastroenterol Hepatol*. 2013;9:711–717.
3. Hall AB, Tolonen AC, Xavier RJ. Human genetic variation and the gut microbiome in disease. *Nat Rev Genet*. 2017;18:690–699. <https://doi.org/10.1038/nrg.2017.63>.
4. Chu H, Khosravi A, Kusumawardhani IP et al. Gene-microbiota interactions contribute to the pathogenesis of inflammatory bowel disease. *Science*. 2016;352:1116–1120. <https://doi.org/10.1126/science.aad9948>.
5. Meddens CA, van der List ACJ, Nieuwenhuis EES, Mokry M. Non-coding DNA in IBD: from sequence variation in DNA regulatory elements to novel therapeutic potential. *Gut*. 2019;68:928–941. <https://doi.org/10.1136/gutjnl-2018-317516>.
6. Li D, Achkar JP, Haritunians T et al. A Pleiotropic Missense Variant in SLC39A8 Is Associated With Crohn's Disease and Human Gut Microbiome Composition. *Gastroenterology*. 2016;151:724–732. <https://doi.org/10.1053/j.gastro.2016.06.051>.
7. Sunuwar L, Frkatović A, Sharapov S, et al. Pleiotropic ZIP8 A391T implicates abnormal manganese homeostasis in complex human disease. *JCI Insight*. 2020;5(20). <https://doi.org/10.1172/jci.insight.140978>
8. Pickrell JK, Berisa T, Liu JZ, Ségurel L, Tung JY, Hinds DA. Detection and interpretation of shared genetic influences on 42 human traits. *Nat Genet*. 2016;48:709–717. <https://doi.org/10.1038/ng.3570>.
9. Nakata T, Creasey EA, Kadoki M et al. A missense variant in SLC39A8 confers risk for Crohn's disease by disrupting manganese homeostasis and intestinal barrier integrity. *Proc Natl Acad Sci*. 2020;117:28930–28938. <https://doi.org/10.1073/pnas.2014742117>.
10. Jumper J, Evans R, Pritzel A et al. Highly accurate protein structure prediction with AlphaFold. *Nature*. 2021;596:583–589. <https://doi.org/10.1038/s41586-021-03819-2>.
11. Bin BH, Seo J, Kim ST. Function, Structure, and Transport Aspects of ZIP and ZnT Zinc Transporters in Immune Cells. *J Immunol Res*. 2018;2018:9365747. <https://doi.org/10.1155/2018/9365747>.
12. Richardson JB, Dancy BCR, Horton CL et al. Exposure to toxic metals triggers unique responses from the rat gut microbiota. *Sci Rep*. 2018;8:6578. <https://doi.org/10.1038/s41598-018-24931-w>.
13. Pajarillo EAB, Lee E, Kang DK. Trace metals and animal health: Interplay of the gut microbiota with iron, manganese, zinc, and copper. *Anim Nutr Zhongguo Xu Mu Shou Yi Xue Hui*. 2021;7:750–761. <https://doi.org/10.1016/j.aninu.2021.03.005>.
14. Douglas GM, Maffei VJ, Zaneveld JR et al. PICRUSt2 for prediction of metagenome functions. *Nat Biotechnol*. 2020;38:685–688. <https://doi.org/10.1038/s41587-020-0548-6>.
15. Jacobs JP, Lin L, Goudarzi M et al. Microbial, metabolomic, and immunologic dynamics in a relapsing genetic mouse model of colitis induced by T-synthase deficiency. *Gut Microbes*. 2017;8:1–16. <https://doi.org/10.1080/19490976.2016.1257469>.
16. Erben U, Loddenkemper C, Doerfel K et al. A guide to histomorphological evaluation of intestinal inflammation in mouse models. *Int J Clin Exp Pathol*. 2014;7:4557–4576.
17. *Investigating Intestinal Inflammation in DSS-Induced Model of IBD*; 2012. <https://doi.org/10.3791/3678>
18. Wirtz S, Neufert C, Weigmann B, Neurath MF. Chemically induced mouse models of intestinal inflammation. *Nat Protoc*. 2007;2:541–546. <https://doi.org/10.1038/nprot.2007.41>.
19. Tong M, Jacobs JP, McHardy IH, Braun J. Sampling of intestinal microbiota and targeted amplification of bacterial 16S rRNA genes for microbial ecologic analysis. *Curr Protoc Immunol*. 2014;107:7.41.1–7.41.11. <https://doi.org/10.1002/0471142735.im0741s107>
20. Mallick H, Rahnavard A, McIver LJ et al. Multivariable association discovery in population-scale meta-omics studies. *PLoS Comput Biol*. 2021;17:e1009442. <https://doi.org/10.1371/journal.pcbi.1009442>.
21. Sharma A, Szymczak S, Rühlemann M et al. Linkage analysis identifies novel genetic modifiers of microbiome traits in families with inflammatory bowel disease. *Gut Microbes*. 2022;14:2024415. <https://doi.org/10.1080/19490976.2021.2024415>.
22. Bubier JA, Chesler EJ, Weinstock GM. Host genetic control of gut microbiome composition. *Mamm Genome*. 2021;32:263–281. <https://doi.org/10.1007/s00335-021-09884-2>.
23. Cohen LJ, Cho JH, Gevers D, Chu H. Genetic Factors and the Intestinal Microbiome Guide Development of Microbe-Based Therapies for Inflammatory Bowel Diseases. *Gastroenterology*. 2019;156:2174–2189. <https://doi.org/10.1053/j.gastro.2019.03.017>.
24. Liu H, Gao P, Jia B, Lu N, Zhu B, Zhang F. IBD-Associated Atg16L1T300A Polymorphism Regulates Commensal Microbiota of the Intestine. *Front Immunol*. 2022;12. <https://doi.org/10.3389/fimmu.2021.772189>
25. Braun T, Di Segni A, BenShoshan M, et al. Individualized Dynamics in the Gut Microbiota Precede Crohn's Disease Flares. *Am J Gastroenterol*. 2019;114(7):1142–1151. <https://doi.org/10.14309/ajg.000000000000136>
26. Nebert DW, Liu Z. SLC39A8 gene encoding a metal ion transporter: discovery and bench to bedside. *Hum Genomics*. 2019;13:51. <https://doi.org/10.1186/s40246-019-0233-3>.
27. Anzaldi LL, Skaar EP. Overcoming the heme paradox: heme toxicity and tolerance in bacterial pathogens. *Infect Immun*. 2010;78:4977–4989. <https://doi.org/10.1128/IAI.00613-10>.
28. Dai J, Yang X, Yuan Y et al. Toxicity, gut microbiota and metabolome effects after copper exposure during early life in SD rats. *Toxicology*. 2020;433–434:152395. <https://doi.org/10.1016/j.tox.2020.152395>.
29. Chi L, Gao B, Bian X, Tu P, Ru H, Lu K. Manganese-induced sex-specific gut microbiome perturbations in C57BL/6 mice. *Toxicol Appl Pharmacol*. 2017;331:142–153. <https://doi.org/10.1016/j.taap.2017.06.008>.
30. Ippolito JR, Piccolo BD, Robeson MS et al. Iron deficient diets modify the gut microbiome and reduce the severity of enteric infection in a mouse model of S. Typhimurium-induced enterocolitis. *J Nutr Biochem*. 2022;107:109065. <https://doi.org/10.1016/j.jnutbio.2022.109065>.
31. Koren O, Tako E. Chronic Dietary Zinc Deficiency Alters Gut Microbiota Composition and Function. *Proceedings*. 2020;61(1). <https://doi.org/10.3390/IECN2020-06993>
32. Chandransu P, Rensing C, Helmann JD. Metal homeostasis and resistance in bacteria. *Nat Rev Microbiol*. 2017;15:338–350. <https://doi.org/10.1038/nrmicro.2017.15>.
33. Gálvez-Peralta M, Wang Z, Bao S, Knoell DL, Nebert DW. Tissue-Specific Induction of Mouse ZIP8 and ZIP14 Divalent Cation/Bicarbonate Symporters by, and Cytokine Response to, Inflammatory Signals. *Int J Toxicol*. 2014;33:246–258. <https://doi.org/10.1177/1091581814529310>.
34. Forster SC, Clare S, Beresford-Jones BS et al. Identification of gut microbial species linked with disease variability in a widely used mouse model of colitis. *Nat Microbiol*. 2022;7:590–599. <https://doi.org/10.1038/s41564-022-01094-z>.

Publisher's Note Springer Nature remains neutral with regard to jurisdictional claims in published maps and institutional affiliations.